Volume 20
Number 1

June *2018*
(ISSN 1109-1606)

Journal of

APPLIED ELECTROMAGNETISM

JAE

Trans Black Sea Region Union of Applied Electromagnetism
BSUAE

Institute of Communication and Computer Systems

Athens - GREECE

Volume 20 **June 2018**
Number 1 **(ISSN 1109-1606)**

JOURNAL
OF
APPLIED ELECTROMAGNETISM

Institute of Communication and Computer Systems

Athens - GREECE

Volume 20 **Number 1**

June 2018

TRANS BLACK SEA REGION UNION OF APPLIED ELECTROMAGNETISM (BSUAE)

JOURNAL OF APPLIED ELECTROMAGNETISM

Institute of Communication and Computer Systems

Athens - GREECE

Journal of Applied Electromagnetism

Copyright Form

The undersigned I confirm that I agree to the publication of the article:

in the Journal of Applied Electromagnetism and the copyright to belong to Trans Black Sea Union of Applied Electromagnetism. I understand that I have the full right to reuse this manuscript for my own purposes.

Name:

Surname:

Address:

E-mail:

Signed:

***Please send the previous form signed either by e-mail to pfrangos@central.ntua.gr , or by fax to the fax number: +30 210 772 2281, attention of Prof. P. Frangos.**

Address

Institute of Communication and Computer Systems,

National Technical University of Athens,

9, Iroon Polytechniou Str.,

157 73 Athens - GREECE

Tel: (+30) 210 772 3694

Fax: (+30) 210 772 2281, attention of Prof. P. Frangos

e-mail: pfrangos@central.ntua.gr

Web site: **http://jae.ece.ntua.gr**

TRANS BLACK SEA REGION UNION OF APPLIED ELECTROMAGNETISM (BSUAE)

JOURNAL OF APPLIED ELECTROMAGNETISM (JAE)

Volume 20 Number 1 June 2018

CONTENTS

outside, at 450 MHz, 900 MHz and 1800 MHz frequencies. The problems are solved using the Method of Auxiliary Sources (MAS). The numerical results showed the presence of resonance phenomena and high reactive field (standing waves) in several scenarios, that causes higher SAR in human tissues and could be dangerous for a human.

HEALTHY AND DISEASED HUMAN BRAIN PROCESSING (short paper)

Ketevan Kotetishvili*, Anna Gogishvili**, Nino Kobalia***

Georgian Technical University (GTU)
0175, 77, M. Kostava str., Tbilisi, Georgia

*Professor, GTU, Faculty of Informatics & Control Systems,
0177, 20, Chikovani Str., Tbilisi, Georgia, ketinooo@hotmail.com

** Engineering Physics Department, Medical Physics Master's Program,
0175, 77 Merab Kostava Str., anuka1@yahoo.com

***Doctoral Researcher, Institute of Neuroscience and Medicine 4,
Forschungszentrum Juelich, Jülich, Germany, n.kobalia@fz-juelich.de

Abstract

After scanning the patient, the data processing presented here follows. First, we must convert 'Dicom' files to 'nifti' files. Then, we need eddy correction (movement to correct distorted photos). After this we use B vectors correction and use MATLAB program, also we use MATLAB for PI, which means background noise correction. For masking we use FSL program, in order to obtain a correct size of brain and finally we use 'MainExploreDTI' to see the direction of fibers.

1. INTRODUCTION

This article describes the basic principles of brain tissue post processing and provides to overview the steps that was necessary, what program we need, such as MATLAB, FSL, Explore DTI program. These examples were illustration to compare each parameter to each other's, what was differences and what was same and see tractography map to show the directions of fibers, which helped us identify if everything was fine or were any pathology of brain.

2. EXPERIMENTAL SET-UP

Human brains are surrounded by a system of connective tissue membranes called meninges that separate the brain from the skull. Brain is made up of white and gray

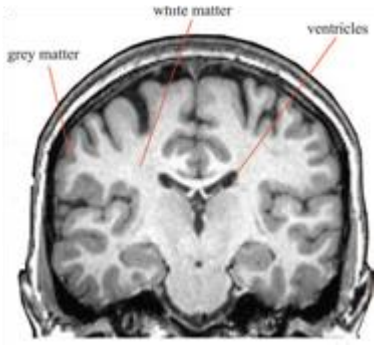

matter and water. Grey matter (or gray matter) is a major component of the central nervous system, consisting of neuronal cell bodies, neuropil (dendrites and myelinated as well as unmyelinated axons), glial cells (astroglioma and oligodendrocytes), synapses, and capillaries. White matter refers to areas of the central nervous system that are mainly made up of myelinated axons also called tracts, white matter actively affects learning and brain functions, modulating the distribution of action potentials.

```
vol0007.nii.gz vol0008.nii.gz vol0009.nii.gz $PE2_b0`
`rm vol*`
#========== prepare the acqparams.txt file ==========
# edit the number of lines according to the number of nonDW
# the echo spacing must be in seconds! (FoV matrix size -1)*
`printf "0 1 0 0.049\n 0 1 0 0.049\n 0 1 0 0.049\n 0 1 0 0.0
\n -1 0 0 0.049\n" > acqparams.txt`

#==================== run topup ====================
`${FSLDIR}/bin/topup --imain=A2P_R2L_b0 --datain=acqparams.t

#========== mean of b0 and mask the result =========
`${FSLDIR}/bin/fslmaths my_hifi_b0.nii.gz -Tmean my_hifi_b0.
`${FSLDIR}/bin/bet my_hifi_b0.nii.gz my_hifi_b0_brain.nii.gz

# ========== prepare the index file ===============
# ---- edit the number of volumes accordingly ------
indx=""
for ((i=1; i<=150; i+=1)); do indx="$indx 1"; done
echo $indx > index.txt

#==================== run eddy ====================
`${FSLDIR}/bin/eddy --imain=$PE1_DWI --mask=my_hifi_b0_brain
_bvecs --bvals=${PE1_DWI:0:${#PE1_DWI}-4}.bvals --topup=my_t
```

Correction of Eddy-Current Distortions in Diffusion Tensor Images Using the Known Directions and Strengths of Diffusion Gradients. To run Eddy correction, we need the scripts for FSL program

After B vector correction, we get FSL files and use FSL program to see the result to calculate the brain information. Now we need 8 maps for this experiment. For example, FA (fractional anisotropy), FA- reflects the directionality of molecular displacement by diffusion and vary between 0 (isotropic diffusion) and 1 (infinite anisotropic diffusion). SD (standard deviation), SD- standard deviation is a measure that is used to quantify the amount of variation or dispersion of a set of data values. MD (mean diffusivity), MD- reflects the average magnitude of molecular displacement by diffusion. The more the MD value, the more the isotropic is the medium, RD (radial diffusivity), RK (radial kurtosis), MK (mean kurtosis.), MK- kurtosis is a measure of the "tailedness" of the probability distribution of a real-valued random variable), AK (axial kurtosis), KA (kurtosis anisotropy).

This data helps us to find the intensity of the program is working. All data have several varying intensities, according to which we encounter any problem in the brain or not. Three types of brain substance: white, gray and white water intensive.

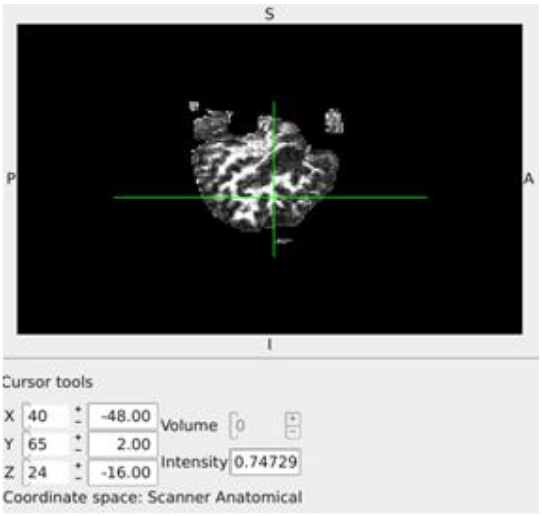

Figure 1. FA map with white matter, with intensity values.

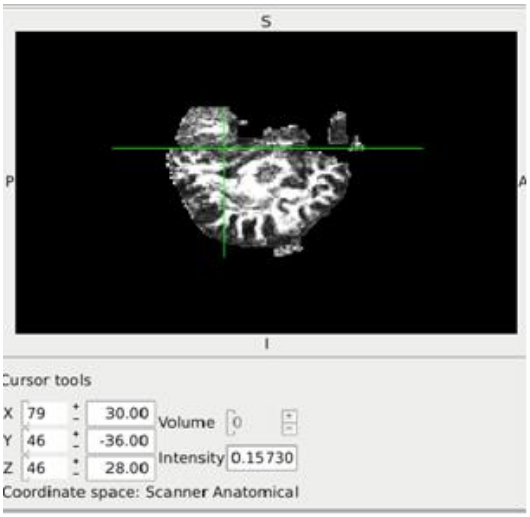

Figure 2. FA map with grey matter, with intensity values.

White matter contains only the myelinated axon tracts and not the cell bodies. It connects various GM regions and carry nerve impulses between neurons. The high density of axons package, low permeability of myelin sheaths, presence of microtubules inside axons and some other factors in hence the motion of water inside the white matter.

Grey matter consists mainly of neuronal cell bodies, dendrites and unmyelinated axons. Dendrites and unmyelinated axons give rise to the restrictions and local anisotropies for diffusion in GM. White substance intensity is high, and decreases of gray water are being reduced.

This is the normal list for intensity values, what maps would have to have in normal tissue.

FA - (0 – 1,5) MD - (10 ^ -3)

KA - (0 – 1,5) MK - (0 – 3)

If these numbers are different it means that, there is some pathology in the brain and are starting to solve this problem.

Here are eight different maps of the healthy human brain contrast. Each map provides a variety of information. Each map is chosen according to the purpose. In our case, we used this map for demonstration.

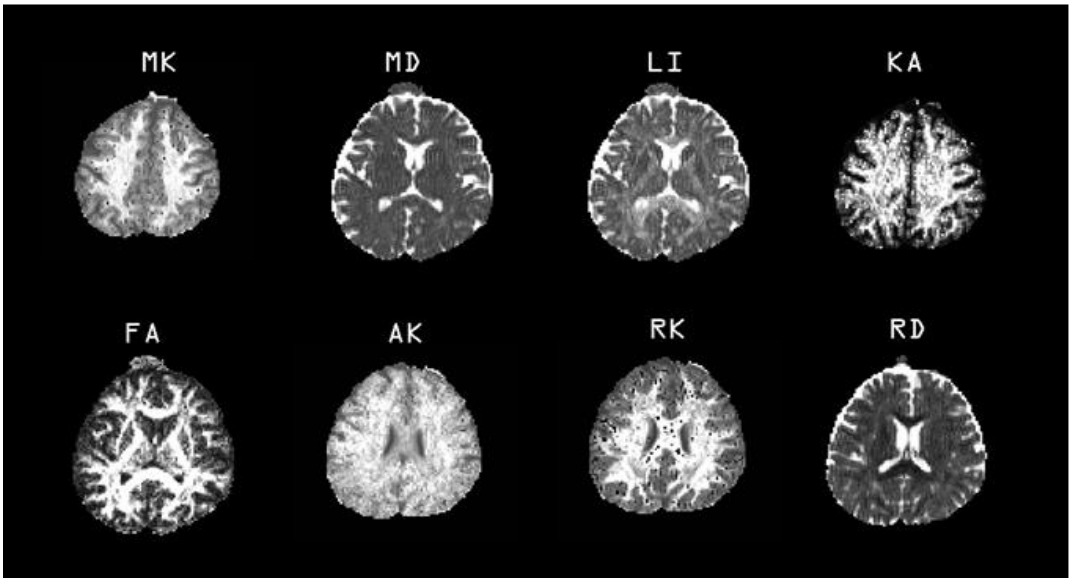

These maps provide MD and MK mapping in vivo human brain. First line represented one patient highest tumor intensity region of the mass on MD and MK maps. There is swelling around the tumor which operates ventricle and changes its form, cannot be said of the healthy human brain.

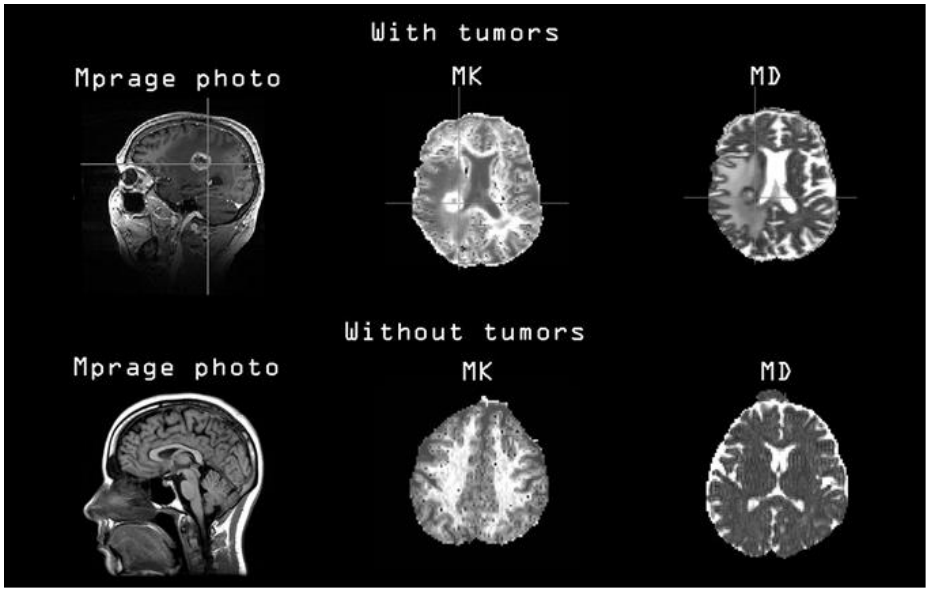

Diffusion Magnetic Resonance Imaging in Brain Tissue

Axons are typically microscopic in diameter (about 1 m across) and have various length from 1 mm to several sm. Axons compound together form threadlike structures called tracts, which in composition with blood vessels surrounded by the epineurium form nerve fibers. Fibers connect one part of the nervous system with another. A neural pathway that function as a connection between relatively distant areas of the brain is known collectively as white matter (WM), and neural pathways that span a shorter distance between structures is called grey matter.

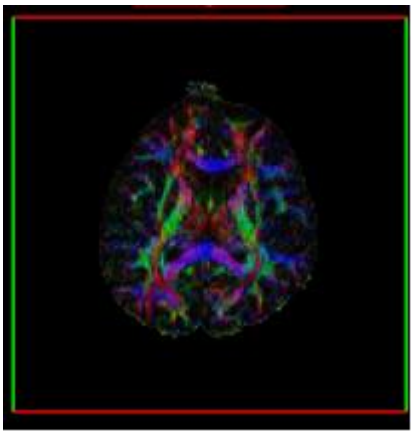

Figure 3. Main DTI metrics

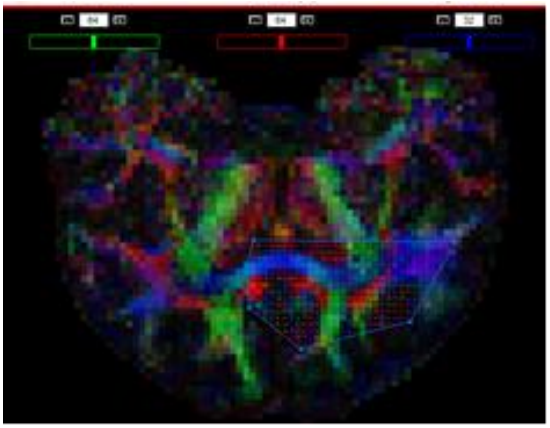

Figure 4. Main DTI metrics

Tensor field was produced with the help of Explore DTI software. Additional advantage of the DTI model is the ability to relate the eigenvector, associated with the maximal eigenvalue, with the preferential fibred track orientation in the voxel. Connecting these local orientations of eigenvectors along adjacent voxels, one can reconstruct the main axis of fibre track trajectory. This technique, called fibre tractography, has been used to study white matter connectivity in the brain, muscle composition, and, since recently, plays a certain role in surgery planning.

3. CONCLUSION

This article was to introduce the stages, that need patient post processing, to compare tumor brain maps with healthy human brain, and to see eight maps for illustration and creative maps with direction of the fibers.

REFERENCES

[1] K.Kotetishvili, N.Kobalia, F.Grinber and E.Farrher, 'Pilot Study of the Correlations Between the Optimism Bias and Brain Microstructure as revealed by DTI Metrics', INM Retreat 2015, Juelich, Germany, 2015.

[2] Scott A. Huettel, Allen W.Song and Gregory McCarthy, 'Functional Magnetic Resonance Imaging', p.573, Duke University, Massachusetts, USA, 2014.

[3] Scott H. Faro and Feroze B. Mohamed, 'Functional MRI : Basic Principles and Clinical Applications', Springer, 2007.

[4] F. Grinberg, E.Farrher, and J. Shah, 'Spatially variable Rician noise in Magnetic Resonance Imaging', Medical Image Analysis (16), pp. 536-548, 2012.

EVALUATING THE INFLUENCE OF CRANIOTOMY ON CORTICAL THICKNESS IN TRAUMATIC BRAIN INJURY USING MAGNETIC RESONANCE IMAGING

(short paper)

Ketevan V. Kotetishvili*, Elene K. Iordanishvili**, Sopho ZH. Mikiashvili***

Georgian Technical University (GTU)
0175, 77, M. Kostava str., Tbilisi, Georgia

*Professor, GTU, Faculty of Informatics & Control Systems,
0177, 20, Chikovani Str., Tbilisi, Georgia, ketinooo@hotmail.com

** MD, PhD student, GTU, Faculty of Informatics & Control Systems, 0194, 22, Bakhtrioni st., ap. 45, Tbilisi, Georgia

*** MD, PhD, Radiology Department, Aversi Clinic, 0160, 27b, Vazha Pshavela Ave, Tbilisi, Georgia

Abstract

While craniotomy is one of the management methods for traumatic brain injury (TBI), there is still controversy about the quality of life and the improved outcome is questioned after this procedure. Present article attempts to evaluate the structural changes of grey matter between the traumatic brain injury patients with and without craniotomy. Utilizing magnetic resonance data and performing voxel-based morphometry, revealed the lower cortical thickness in TBI patients with craniotomy compared to their non-craniotomy counterparts.

1. INTRODUCTION

Traumatic brain injury (TBI) is one of the leading causes of disability and death worldwide. It represents a high socio-economic burden for the society [1]. Even the minor insult can be the reason of cognitive and behavioral impairment [2]. A wide range of treatment strategies exists for coping with this devastating pathology, starting from pharmacological management, continuing with surgical intervention [3]. While

craniotomy is frequently used for managing high intracranial pressure to avoid secondary brain injury, research papers are still full of controversy about the quality of life and question the improved outcome after this procedure [4-6].

Either short or long-term cognitive dysfunction is a well-known attribute of traumatic brain injury [7]. Normal mental performance is one of the measures of the outcome in TBI patients. The structural marker for cognitive decline is grey matter atrophy. Multiple authors have reported cortical thinning after traumatic brain injury, even in mild cases [8-10]. To the best of our knowledge, whether craniotomy itself exaggerates the process has not been investigated yet.

The aim of our study was to explore the effect of craniotomy on cortical atrophy in TBI. For this purpose, we retrospectively retrieved the TBI patients' data with and without craniotomy and analyzed their Magnetic Resonance Images (MRI) using voxel-based morphometry.

2. MATERIALS AND METHODS

2.1. Subjects

Twelve TBI patients' data was retrieved and anonymized from the radiology department of Aversi Clinic. Medical histories were checked to exclude other central nervous system pathologies. Three of them were dropouts due to congenital brain anomalies and one was below the age of 18. From the remaining eight patients, three of them had undergone craniotomy. Patients ranged from moderate to severe cases and all of them were measured in the chronic phase of injury. In Craniotomy group two was male and one female with mean age: 32±7.55. Non-craniotomy group presented with three male and one female. Mean age was 40.2±13.48.

2.2. MRI data acquisition

Images were acquired on 1.5 tesla Philips scanner. High resolution 3D T1 weighted Fast field echo (FFE) images were acquired in the sagittal plane. Repetition time/echo time (TR/TE) = 3.77/1.7ms. Flip angle = 8. Number of echoes = 1. Echo train length = 425. Voxel size = 0.98X0.98mm. Slice thickness = 2.2mm.

2.3. Data post processing and analysis

The MRI data was visually inspected for the motion artifacts. The T1weighted images were processed using Computational Anatomy Toolbox (CAT12) within SPM12 in MATLAB_R2015a. Images were registered to Montreal Neurological Institute standard space. Then skull-stripping, bias-field correction and tissue classification into grey, white matter (GM, WM) and cerebro-spinal fluid (CSF) was performed. Cortical thickness was measured for each patient and the tissue segmentations were modulated by scaling with the amount of volume changes caused by spatial registration [11].

Voxel-based morphometry (VBM) was done and cortical thickness was measured for all subjects. VBM provides the voxel-wise estimation of the specific tissue compartment's local amount or volume [12]. Finally, two-sample t-test was performed to evaluate the local cortical changes between TBI patients with and without craniotomy. In order to compare grey matter concentration in different groups, we used the threshold of p value=0.001 (uncorrected) and minimum 20 voxels in a cluster. Total intracranial volume was calculated and considered in the statistical model with age and gender.

3. RESULTS

Craniotomy group of patients showed lower total cortical thickness compared to non-craniotomy counterparts, even though the mean age of the later was higher [See figure 1]. And cortical thickness is known to decrease with age [13].

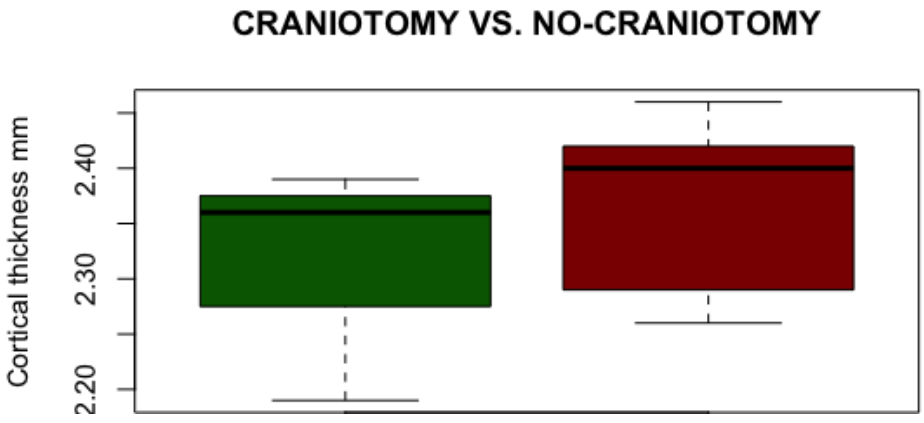

Figure 1. Green boxplot represents the group of craniotomy patients and red – without craniotomy. The horizontal black line indicates the median and the whiskers extend to the upper and lower values.

Two-sample t-test revealed three clusters showing atrophy in craniotomy patients compared to non-craniotomy ones [See figure 2]. After overlaying them to the Montreal Neurological Institute atlas, one of the regions was identified to be in the right precuneus and two of them close to each other in the lingual gyrus of the left occipital lobe.

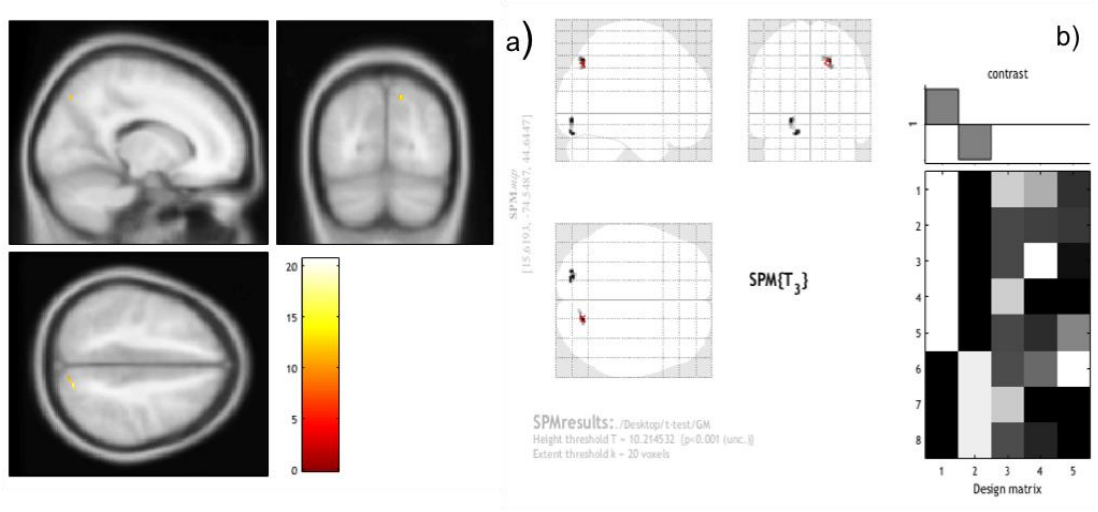

Figure 2. a) The results of two-sample t-test is overlaid to MNI 152 and depicts one of the clusters of difference between the groups, b) Design matrix with two groups (group1 = without craniotomy, group2 = craniotomy), gender, age and total intracranial volume are considered into the statistical model as covariates. Three clusters are shown on the brain mask.

4. CONCLUSIONS AND DISCUSSIONS

This study showed that traumatic brain injury patients with craniotomy are more prone to cortical thinning compared to their counterparts without surgery. Local cerebral regions, in particular precuneus and lingual gyrus, which showed atrophy, are involved in the episodic memory retrieval and visual memory encoding [14-15]. Cortical atrophy and cognitive deficit is a well-known sequel of TBI [16,17]. Whether craniotomy exaggerates this process, is not truly established. Arciniegas et al. evaluated cognitive performance as a function of conservative treatment [18]. Our study evaluated cortical thickness with relation to craniotomy in TBI patients as a structural marker of cognitive dysfunction.

The strength of the study is an interesting cohort, but limitation is the small subject number. Another limitation is diversity of trauma, ranging from moderate to severe. In the future studies, it is recommended to include more homogeneous cohort.

ACKNOWLEDGEMENT

This work was supported by Shota Rustaveli National Science Foundation (Aleksidze Str. #1, Tbilisi, Georgia, info@rustaveli.org.ge http://rustaveli.org.ge) in the frame of the PhD Scholarship. The authors thank to Aversi Clinic ltd. and its Radiology Department, in particular Dr. Dina Tskhvaradze, Dr. Irakli Gakhokidze, Dr. Magda Tsirekidze, Dr. Maia Apriamashvili, Dr. Sophio Chkhenkeli, and Dr. Natia Tugushi for fruitful discussions upon the clinical cases.

REFERENCES

[1] Peeters, W., van den Brande, R., Polinder, S., Brazinova, A., Steyerberg, E. W., Lingsma, H. F., & Maas, A. I. R. (2015). Epidemiology of traumatic brain injury in Europe. Acta Neurochirurgica, 157(10), 1683–1696.

[2] Miotto, E. C., Cinalli, F. Z., Serrao, V. T., Benute, G. G., Lucia, M. C. S., Scaff, (2010). Cognitive deficits in patients with mild to moderate traumatic brain injury. Arquivos de Neuro-Psiquiatria, 68(6), 862–868.

[3] Carney, N., Totten, A. M., O'Reilly, C., Ullman, J. S., Hawryluk, G. W. J., Bell, M. J., … Ghajar, J. (2016). Guidelines for the Management of Severe Traumatic Brain Injury, Fourth Edition. Neurosurgery, (September).

[4] Howard JL, Cipolle MD, Anderson M, et al. Outcome after decompressive craniectomy for the treatment of severe traumatic brain injury. J Trauma. 2008;65(2):380–385.

[5] Kolias A.G., Kirkpatrick PJ, Hutchinson PJ. Decompressive craniectomy: past, present and future. Nat Rev Neurol. 2013;9(7):405–415.

[6] Jiang JY, Xu W, Li WP, et al. Efficacy of standard trauma craniectomy for refractory intracranial hypertension with severe traumatic brain injury: a multicenter, prospective, randomized controlled study. J Neurotrauma. 2005;22(6):623–628.

[7] Moretti, L., Cristofori, I., Weaver, S. M., Chau, A., Portelli, J. N., & Grafman, J. (2012). Cognitive decline in older adults with a history of traumatic brain injury. The Lancet. Neurology, 11(12), 1103–12.

[8] MacKenzie, J. D., Siddiqi, F., Babb, J. S., Bagley, L. J., Mannon, L. J., Sinson, G. P., & Grossman, R. I. (2002). Brain atrophy in mild or moderate traumatic brain injury:

a longitudinal quantitative analysis. AJNR. American Journal of Neuroradiology, 23(9), 1509–1515.

[9] Gale, S. D. (2005). Traumatic brain injury and grey matter concentration: a preliminary voxel based morphometry study. Journal of Neurology, Neurosurgery & Psychiatry, 76(7), 984–988.

[10] Cole, J. H., Leech, R., & Sharp, D. J. (2015). Prediction of brain age suggests accelerated atrophy after traumatic brain injury. Annals of Neurology, 77(4), 571–581.

[11] C. Gaser, R. Dahnke (2016). CAT - A Computational Anatomy Toolbox for the Analysis of Structural MRI Data. HBM 2016.

[12] J. Ashburner (2005): Unified segmentation. Neuroimage 26(3):839-51.

[13] Fjell, A. M., Grydeland, H., Krogsrud, S. K., Amlien, I., Rohani, D. A., Ferschmann, L., Walhovd, K. B. (2015). Development and aging of cortical thickness correspond to genetic organization patterns. Proceedings of the National Academy of Sciences, 112(50), 15462–15467.

[14] Cavanna, A. E., & Trimble, M. R. (2006). The precuneus: A review of its functional anatomy and behavioural correlates. Brain, 129(3), 564–583.

[15] Duane Heines. (2017). Study guide by Cram 101textbook reviewsNeuroanatomy, An Atlas of Structures, Sections, and Systems: 8th edition.

[16] Bigler, E. D. (2013). Traumatic brain injury, neuroimaging, and neurodegeneration. Frontiers in Human Neuroscience, 7(August), 1–15.

[17] Spitz, G., Bigler, E. D., Abildskov, T., Maller, J. J., O'Sullivan, R., & Ponsford, J. L. (2013). Regional cortical volume and cognitive functioning following traumatic brain injury. Brain and Cognition, 83(1), 34–44.

[18] Archiniegas D.B., Held K., Wagner P. (2002). Cognitive Impairment Following Traumatic Brain Injury. Current Treatment Options in Neurology. 2002 Jan4(1):43-57.

EM EXPOSURE STUDY OF A HUMAN INSIDE THE CAR

(selected from CEMA'17 Conference)

Veriko Jeladze, Tamar Nozadze, Vasil Tabatadze, Ivan Petoev, Revaz Zaridze

Tbilisi State University, Laboratory of Applied Electrodynamics and Radio Engineering

3, Chavchavadze Ave. 0176, Tbilisi, Georgia

Email: veriko.jeladze001@ens.tsu.edu.ge

Email: tamar.nozadze002@ens.tsu.edu.ge

Abstract

The goal of the proposed research is to investigate the influence of mobile phone's EM Radiation on a human, when it is located inside the car and study possible resonant fields in car. We have investigated several cases when a human with a cellphone is located inside a car and also the case when the EM source is the base station antenna located outside, at 450 MHz, 900 MHz and 1800 MHz frequencies. The problems are solved using the Method of Auxiliary Sources (MAS). The numerical results showed the presence of resonance phenomena and high reactive field (standing waves) in several scenarios, that causes higher SAR in human tissues and could be dangerous for a human.

1. INTRODUCTION

Nowadays it's especially important and actual to investigate the impacts of electromagnetic fields (EMF) emitted from the cellphones and other wireless communication devices on human. The interaction between the EMFs and the biological object depends on the characteristics of the emitting source, as well as the ability to absorb and accumulation energy by biological organisms. Many publications show that absorption of radiated energy (SAR) depends on mobile phones and antenna types [1, 2], its positions, and radiated power from the mobile phones [3]. The radiation nature and EM fields behavior depends on complex human body geometry [4], user hand and fingers positions [2, 5], other subjects' existence around the user, etc. It's also important to consider where the user is located, in an enclosed or semi-enclosed space (room, car, etc.). But it's impossible to thoroughly quantitatively consider all these details.

In our previous works [6, 7] we have investigated the cellphone's antenna and base station's radiation influence on the user located inside the room with a window. The studies were conducted by the Method of Auxiliary Sources (MAS), which was also used to simulate room walls with different transparency. The results showed the presence of high reactive fields in the room with less walls transparency [7].

In this paper our goal is to investigate mobile phones antenna EM exposure influence on a human, when person is located inside the car and study possible resonant fields in cars at 900 MHz and 1800 MHz radiation frequencies. The motivation of this research is that we often use mobile phones and other handsets in a car (e.g. walkie-talkies are used in police cars). As it is known, cars are made using metal and other conductive materials, which are less transparent to EM waves. At some frequencies in the mobile frequency range, this closed metal structure behaves as a resonator and amplifies the antenna radiated near field, which becomes dangerous for the user. Besides, the novelty in the proposed research is the ground effect consideration under the car, as a reflective surface. It is also important to study SAR distributions inside the human body and investigate the fields' behavior in the near and far zone.

There are some publications [8-9] similar to the stated problem solved by different numerical methods, but we suppose that, the EMF exposure influence on a human inside the car is not studied completely yet.

2. MATHEMATICAL APPROACH AND METHODOLOGY

We consider the system model which consists of the car and human inside it. The system is irradiated by the known EM wave, which is located inside the car as a mobile phone antenna. Our goal is to find the EMF distribution inside and outside the car and also, inside a human body and also to investigate the earth surface influence on the resonant field formation inside the car. In the considered model (Figure 1) the car represents the perfectly conductor surface S. On these surfaces there are open parts like windows, σ_w, $w = 1, 2, ...$ number of glasses. As a human model we use the homogenous dielectric model of a human shape "Mummy" with averaged permittivity and losses [6], which is bounded with the closed surface S_0.

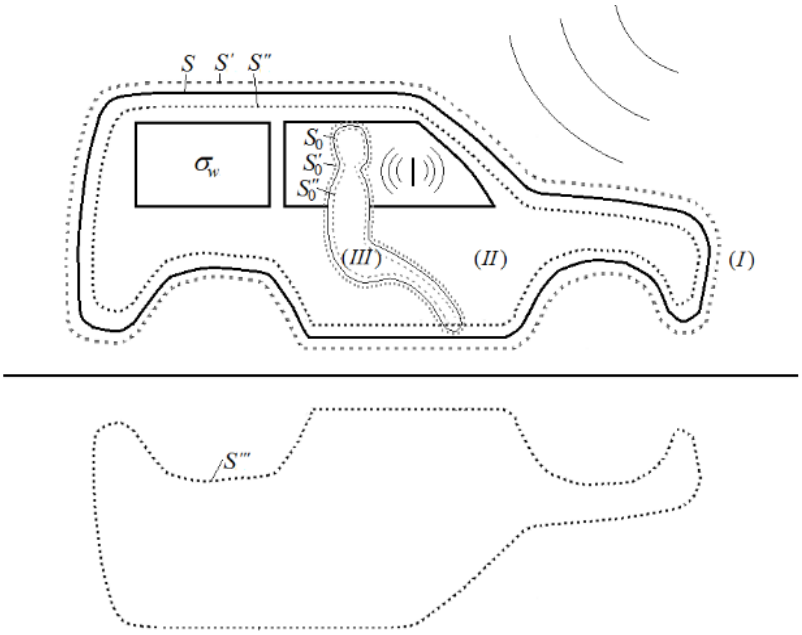

Figure 1. MAS model of cavity with using auxiliary surfaces.

The irradiated fields of the inner source $\vec{E}^1_{inc}, \vec{H}^1_{inc}$ (first case) and the field of the outer source $\vec{E}^2_{inc}, \vec{H}^2_{inc}$ (second case) are initially given. We have to determine the field in three areas: (I) outside the car, (II) inside car, (III) inside human (Figure 1). We denote these fields correspondingly $\vec{E}_{(I)}, \vec{H}_{(I)}$, $\vec{E}_{(II)}, \vec{H}_{(II)}$, $\vec{E}_{(III)}, \vec{H}_{(III)}$. The stated problem is solved numerically, using the Method of Auxiliary Sources (MAS).

For this reason we construct two couples of auxiliary surfaces: S_0', S_0'' - outside and inside human, and S', S'', – outside and inside car, where the auxiliary sources are distributed. As the auxiliary sources two mutual perpendicularly oriented combined dipoles (Huygens source) [10, 11] with unknown amplitudes are used. The electric and magnetic field of the combined dipole is denoted as:

$$\begin{aligned} \vec{G}_E &\to \vec{G}_E\left(\vec{r}, \vec{r}_0, \vec{p}_e, \vec{p}_h, \varepsilon, \mu\right) \\ \vec{G}_H &\to \vec{G}_H\left(\vec{r}, \vec{r}_0, \vec{p}_e, \vec{p}_h, \varepsilon, \mu\right) \end{aligned} \tag{1}$$

where $\vec{r}$ and $\vec{r}_0$ are the observation point and dipole location point radius-vectors, $\vec{p}_e$ and $\vec{p}_h$ are the unit vectors of the electric and magnetic dipole polarization, ε and μ are media parameters. In order to describe the scattered field of any polarization, in each point of the auxiliary surface we consider two such dipoles, distributed in the tangent

plane and rotated by 90° to each other. Respectively, for electric and magnetic field of the auxiliary source we have:

$$A_0\vec{G}_E + B_0\vec{G}'_E \ , \ A_0\vec{G}_H + B_0\vec{G}'_H \tag{2}$$

where: $\begin{matrix}\vec{G}'_E \to \vec{G}_E\left(\vec{r},\vec{r}_0,\vec{p}'_e,\vec{p}'_h,\varepsilon,\mu\right) \ , \ \vec{p}'_e = \vec{p}_h \\ \vec{G}'_H \to \vec{G}_H\left(\vec{r},\vec{r}_0,\vec{p}'_e,\vec{p}'_h,\varepsilon,\mu\right) \ , \ \vec{p}'_h = -\vec{p}_e\end{matrix}$, A_0 , B_0 are unknown complex amplitudes, which can be determined by satisfaction of the corresponding boundary conditions.

The field in the first (I) area is the sum of the incident field, $\vec{E}^1_{inc}, \vec{H}^1_{inc}$ and the field described by the auxiliary sources on the surface S''. The field in the second (II) area is the sum of the incident field, $\vec{E}^2_{inc}, \vec{H}^2_{inc}$ and the fields described by the sources located on the surface S' and S''_0. In the third (III) area the field is described by the sources on the surface S'_0 (Figure 1). Therefore:

$$\vec{E}_{(I)}\left(\vec{r}\right) = \vec{E}^1_{inc}\left(\vec{r}\right) + \sum_{n=1}^{N}\left[A_n\vec{G}_E + B_n\vec{G}'_E\right]_{\vec{r}_n\in S''} \tag{3}$$

$$\vec{E}_{(II)}\left(\vec{r}\right) = \vec{E}^2_{inc}\left(\vec{r}\right) + \sum_{n=1}^{N}\left[C_n\vec{G}_E + D_n\vec{G}'_E\right]_{\vec{r}_n\in S'} + \sum_{m=1}^{N_0}\left[E_m\vec{G}_E + F_m\vec{G}'_E\right]_{\vec{r}_m\in S''_0} \tag{4}$$

$$\vec{E}_{(III)}\left(\vec{r}\right) = \sum_{m=1}^{N_0}\left[K_m\vec{G}_E + L_m\vec{G}'_E\right]_{\vec{r}_m\in S'_0} \tag{5}$$

$$\vec{H}_{(I)}\left(\vec{r}\right) = \vec{H}^1_{inc}\left(\vec{r}\right) + \sum_{n=1}^{N}\left[A_n\vec{G}_H + B_n\vec{G}'_H\right]_{\vec{r}_n\in S''} \tag{6}$$

$$\vec{H}_{(II)}\left(\vec{r}\right) = \vec{H}^2_{inc}\left(\vec{r}\right) + \sum_{n=1}^{N}\left[C_n\vec{G}_H + D_n\vec{G}'_H\right]_{\vec{r}_n\in S'} + \sum_{m=1}^{N_0}\left[E_m\vec{G}_H + F_m\vec{G}'_H\right]_{\vec{r}_m\in S''_0} \tag{7}$$

$$\vec{H}_{(III)}\left(\vec{r}\right) = \sum_{m=1}^{N_0}\left[K_m\vec{G}_H + L_m\vec{G}_H\right]_{\vec{r}_m\in S'_0} \tag{8}$$

In the given expression there are unknown complex amplitudes A_n, B_n , C_n , D_n, E_m, F_m, K_m, L_m of the auxiliary sources, the total number of which is $4\cdot\left(N+N_0\right)$. These amplitudes can be determined from the boundary conditions. On the surface S as on the conductor, the tangent components of the complete fields $\vec{E}_{(I)}$, $\vec{E}_{(II)}$ must be zero; On

the windows surfaces σ_w and human model surface, as on the dielectric, the tangent components of the fields $\vec{E}_{(I)}, \vec{E}_{(II)}, \vec{H}_{(I)}, \vec{H}_{(II)}$ and $\vec{E}_{(II)}, \vec{E}_{(III)}$, $\vec{H}_{(II)}, \vec{H}_{(III)}$ must be continuous. As a result, we get the system of the linear algebraic equations to the unknown amplitudes. After solution of this system using the computer numerically, the unknown fields are determined in all given areas.

As it was mentioned above, the big interest is to investigate the ground surface influence on the field formation. We suppose that the ground surface is perfect planar conductor. This gives ability to use the method of the mirror image in order to describe the reflected field. The consideration of the reflected field adds the additional terms in the expressions (3) and (6) for the field in the first area. As for the fields in the second and third areas the reflected field changes only the amplitudes of the auxiliary sources.

According to the MAS, towards ground there is constructed the mirror image S''' of the surface S'' (Figure 1). The amplitudes of the auxiliary sources on the surface S''' differ from the corresponding sources on the surface S'' only by sign as it is in case of the mirror image. In other words the consideration of the ground surface doesn't change the number of the unknown coefficients. The field in the first area has the form:

$$\vec{E}_{(I)}(\vec{r}) = \vec{E}^1_{inc}(\vec{r}) + \sum_{n=1}^{N}\left[A_n\vec{G}_E + B_n\vec{G}'_E\right]_{\vec{r}_n\in S'''} + \sum_{n=1}^{N}\left[(-A_n)\vec{G}^*_E + (-B_n)\vec{G}'^*_E\right]_{\vec{r}_n\in S'''} \quad (9)$$

$$\vec{H}_{(I)}(\vec{r}) = \vec{H}^1_{inc}(\vec{r}) + \sum_{n=1}^{N}\left[A_n\vec{G}_E + B_n\vec{G}'_E\right]_{\vec{r}_n\in S'''} + \sum_{n=1}^{N}\left[(-A_n)\vec{G}^*_E + (-B_n)\vec{G}'^*_E\right]_{\vec{r}_n\in S'''} \quad (10)$$

The unknown amplitudes are again determined from the boundary conditions.

3. RESULTS OF NUMERICAL SIMULATIONS AND DISCUSSIONS

Based on above proposed methodology (MAS), we have created program package and investigated several exposure scenarios. Calculations were carried out at 900 and 1800 MHz radiation frequencies. EM source is placed at 2.5 cm distance from the human head. The car has following dimensions (LWH): 4.10 x 1.76 x 1.57 [m].

For all results near and far field values are given in the relative units, point SAR values are provided in W/Kg and normalized to 1 W input power.

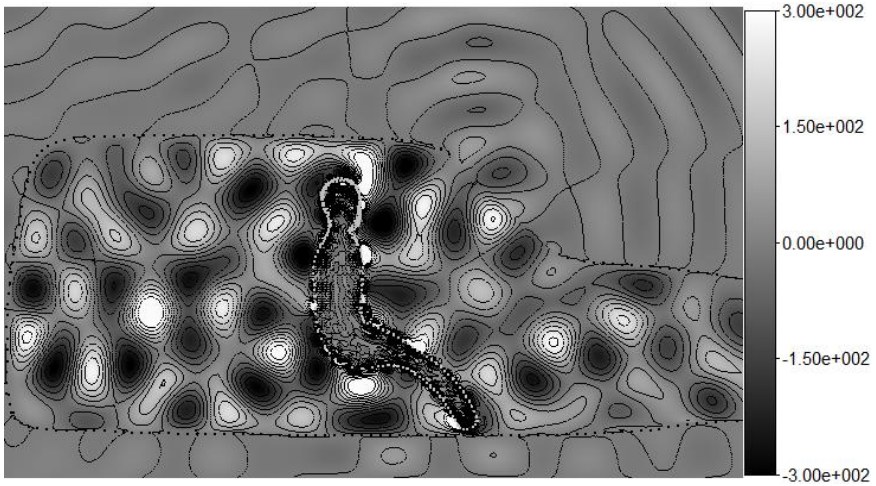

a)

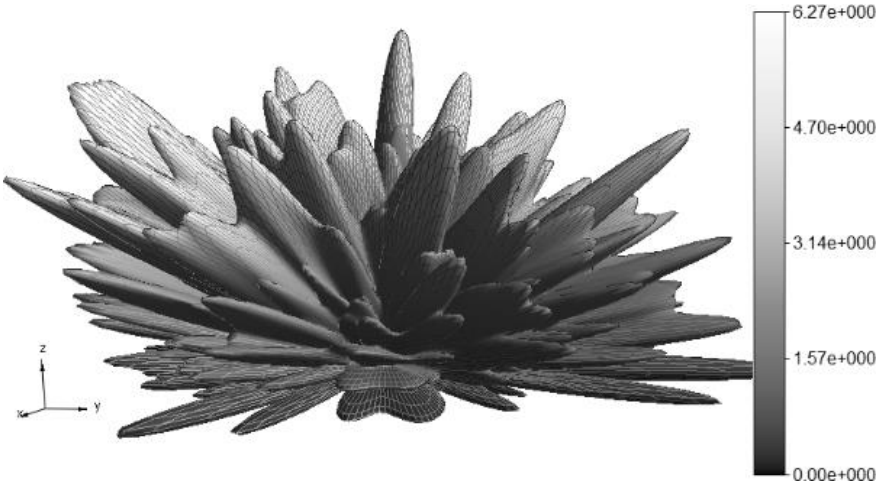

b)

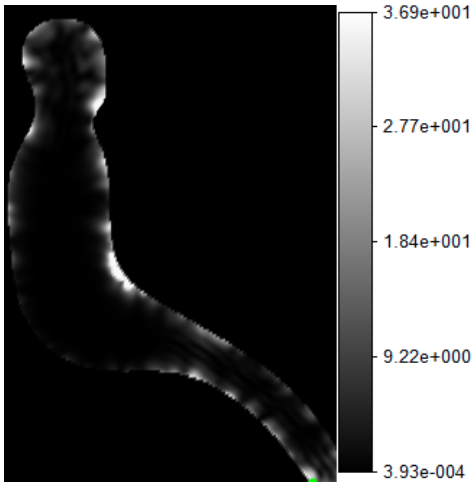

c)

Figure 2. Near field distribution in XOZ plane inside the car (a), far field pattern (b) and point SAR distribution (W/Kg) for the human body (c) at 900 MHz.

On Figures 2 (a, b, c) near field distribution inside the car in XOZ section and far field pattern and point SAR distribution for the human body at 900 MHz frequency are presented respectively. In this case point SAR peak value is 36.9 W/Kg. The wavelength is smaller than car window size and radiated energy penetrates inside the car though the side windows mainly. Standing waves are observed in the back part of car. The bottom of pattern shape is flat, which is caused by the field reflection and propagation over the ground surface under the car.

We have investigated car's resonant properties and generate resonant characteristic near to the 900 MHz frequency. Figure 3 shows the detailed frequency characteristic on which we see the sharp, discriminated resonance frequency 899.9 MHz.

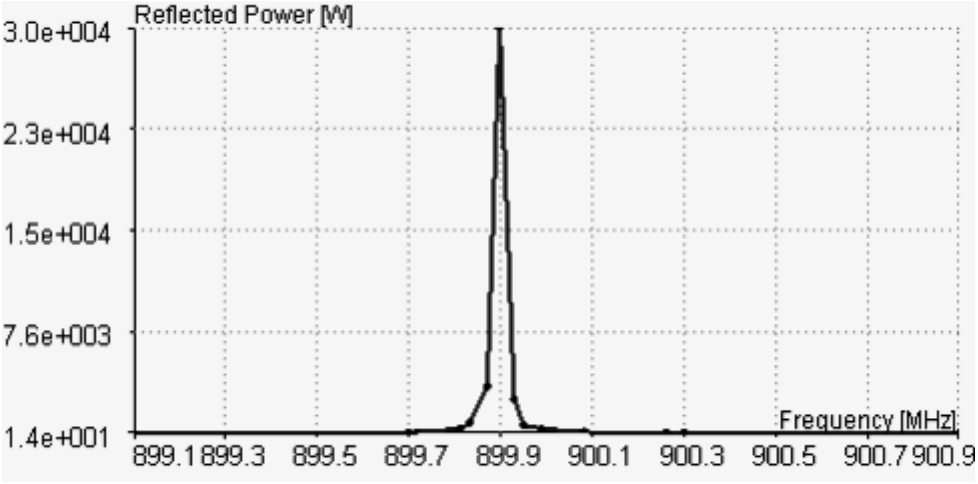

Figure 3. Frequency characteristic for the car with human model inside, near to 900 MHz.

Figure 4 shows near field inside the car (a) and point SAR distribution for the human body (b) at 899.9 MHz resonant frequency. As it seen from the obtained result inside the car is created high reactive field and the point SAR peak value is about ten times higher than it was for the 900 MHz frequency.

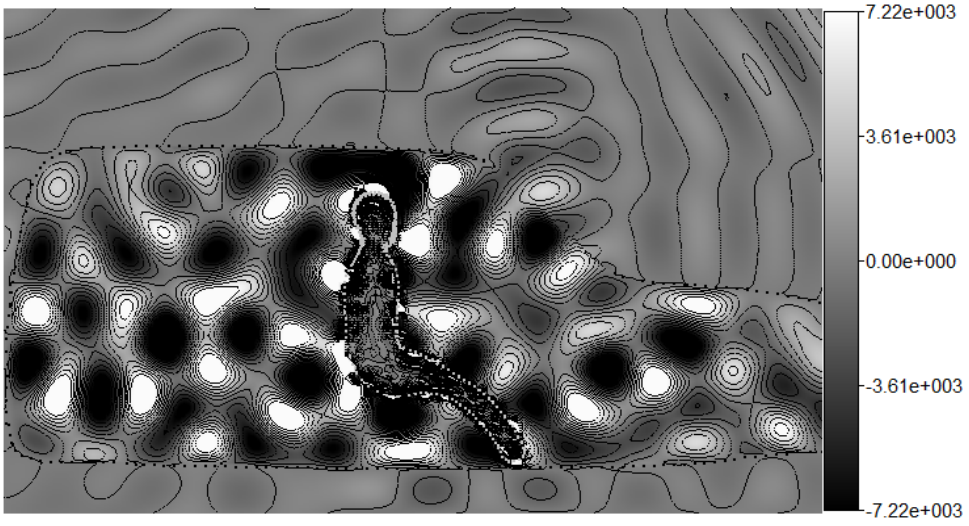

a)

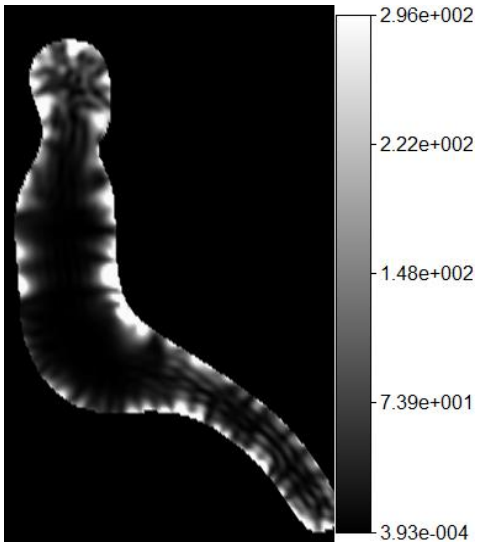

b)

Figure 4. Near filed distribution inside the car (a) and point SAR (b) distribution for the human body at 899.9 MHz resonant frequency.

We have also studied the near field distribution inside the car at 1800 MHz (Figure 5). Because of the high losses at this frequency the depth of the field penetration in the human model is smaller than for the lower frequencies and EM field absorption occurs mostly in the skin layer.

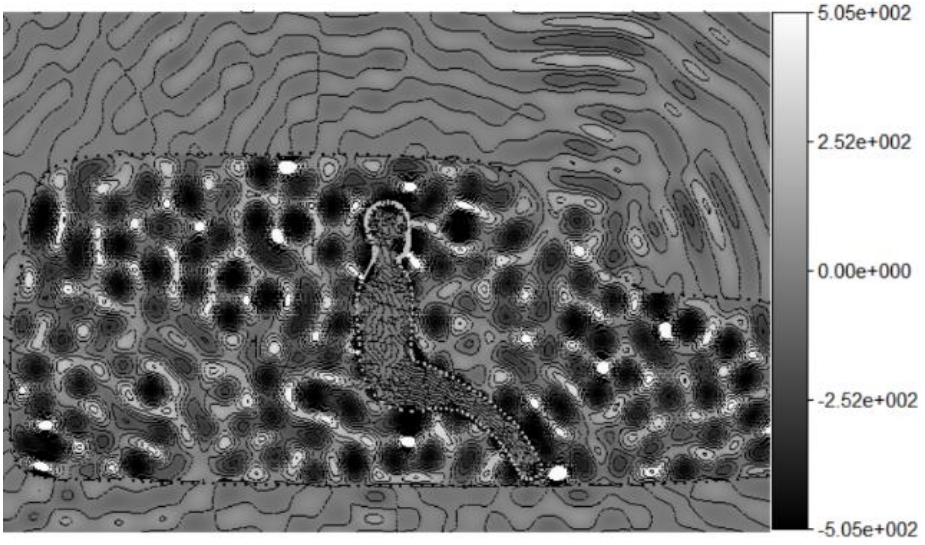

Figure 5. Near field distribution in the car at 1800 MHz frequency (source is base station antenna).

On Figure 6 are presented the SAR values inside the human body, when it is located in free space and in the car, at 450, 900 and 1800 MHz frequencies. We see that in the car these values for the human body is almost 4 times higher than in free space, which can be dangerous for the human.

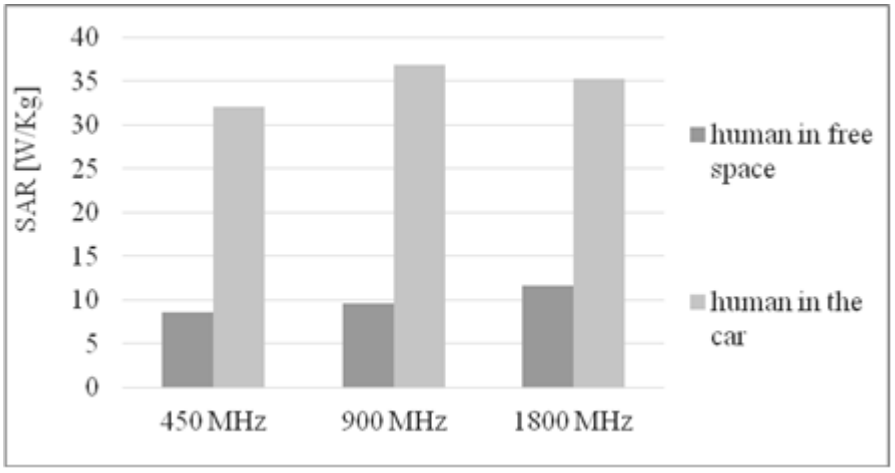

Figure 6. Point SAR values for the human body, when EM source is near the head.

We have also considered the case, when the ground effect under the car isn't taken into account. In this case the field values inside the car are lower (Figure 7) than in the case where we consider this effect (Figure 2a).

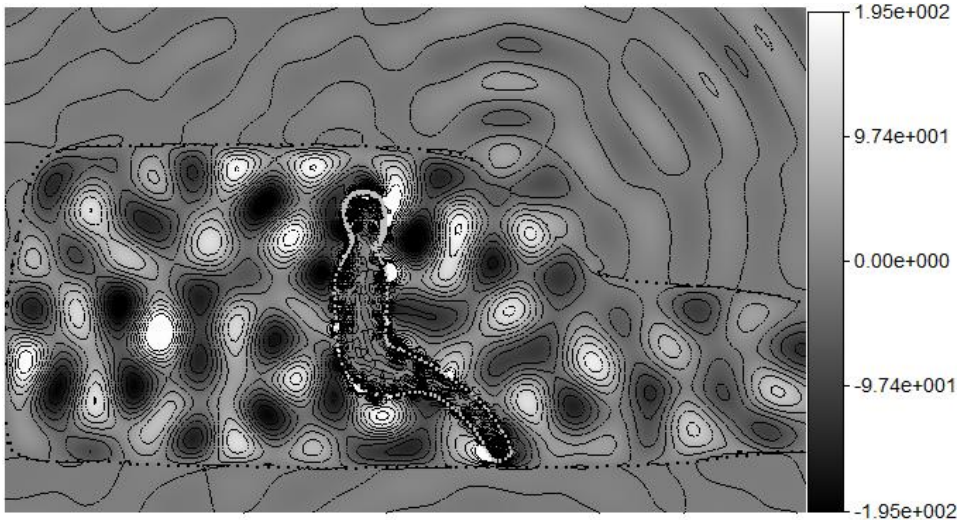

Figure 7. Near field distribution in XOZ plane inside the car without considering ground effect at 900 MHz

For all obtained above results, calculation error was less than 20%.

4. CONCLUSION

The mobile phone's EM exposure problem for a human model located in the car is studied using the Method of Auxiliary Sources. This method was also used to simulate ground reflective surface. The obtained results, conducted with the MAS based program package, showed the presence of resonance and reactive fields inside the car, that causes high SAR in human tissues. It was shown that these SAR values are much higher than in case, when human is in free media. The reason of this is that at the considered frequencies car's metallic surface acts as the resonator. So, it isn't desirable speak on phones for a long time inside the car, that can be hazardous for the cellphone users.

ACKNOWLEDGEMENT

This study is supported by Shota Rustaveli National Science Foundation grant: YS15_2.12_56.

REFERENCES

[1] M. R. I. Faruque, et al.,"Effects of dielectric values & substrate materials on electromagnetic (EM) absorption in human head," Frequenz Journal, vol. 66, no. 3-4, pp. 79-83, 2012.

[2] J. Keshvari & M. Kivento, "Hand Effect on Head Specific Absorption Rate (SAR) Exposed by Two Realistic Phone Models," in Radio and Antenna Days of the Indian Ocean (RADIO 2012), IOP Conf. Series: Materials Science and Engineering, 2012.

[3] J. Wiart et al., "Analysis of the influence of the power control and discontinuous transmission on RF exposure with GSM mobile phone," IEEE Trans. on Electromag. Compat., vol. 42, no. 4, pp. 376-385, 2000.

[4] M. R. I. Faruque, et. al, "Effect of human head shapes for mobile phone exposure on electromagnetic absorption," Journal of Microelectronics, Electronic Components and Materials, vol. 40, no. 3, pp. 232-237, 2010.

[5] V. Jeladze, M. Tsverava, T. Nozadze, et al., "EM Exposure Study on Inhomogeneous Human Model Considering Different Hand Positions," XXI-th Int. Seminar/Workshop on Direct and Inverse Problems of EM and Acoustic Wave Theory (DIPED-2016), Tbilisi, Georgia, September 26-29, 2016.

[6] V. Jeladze, I. Petoev, V. Tabatadze, M. Prishvin, R. Zaridze, "Application of the Method of Auxiliary Sources to Study the Influence of Resonance Electromagnetic Fields on a Man in Large Spatial Domains," Journal of Commun. Technology and Electronics, vol. 62, no. 3, pp. 195-204, March 2017.

[7] V. Jeladze, V. Tabatadze, M. Prishvin, I. Petoev, R. Zaridze, "Influence of the Walls Transparency on the Resonant EM Field's Values," Journal of Applied Electromagnetism (JAE), vol. 18, no. 1, pp. 1-13, June 2016.

[8] G. Anzaldi, et al., "Initial Analysis of SAR from a Cell Phone Inside a Vehicle by Numerical Computation," IEEE Trans. on Biomed. Eng, vol.54, no.5, pp.921-930, May 2007.

[9] A. Dhami, "Studies on Cell-phone Radiation Exposure Inside a Car and Near a Bluetooth Device," Int. J. Environ. Res., vol. 9, no. 3, pp. 977-980, Summer 2015.

[10] В. В. Никольский, Электродинамика и распространение радиоволн, М.: Наука, 1978, p. 221.

[11] I. M. Petoev, V. A. Tabatadze, R. S. Zaridze, "The Me¬thod of Auxiliary Sources Applied to Problems of Electromagnetic Wave Diffraction by Certain Metal–Dielec¬tric Structures," Journal of Commun. Techn. and Electronics, vol. 58, no. 5, pp. 404-416, 2013.